Universal Time and Length Scales of Polar Active Polymer Melts

Universal time and length scales of polar active polymer melts

Mattia Alberto Ubertini,[*,†,¶] Emanuele Locatelli,[*,‡] and Angelo Rosa[*,†]

†*Scuola Internazionale Superiore di Studi Avanzati (SISSA), Via Bonomea 265, 34136 Trieste, Italy*

‡*Department of Physics and Astronomy, University of Padova, Via Marzolo 8, I-35131 Padova, Italy and INFN, Sezione di Padova, Via Marzolo 8, I-35131 Padova, Italy*

¶*Current affiliation: Friedrich Miescher Institute for Biomedical Research (FMI), 4056 Basel, Switzerland*

E-mail: mattia.ubertini@fmi.ch; emanuele.locatelli@unipd.it; anrosa@sissa.it

Abstract

We present an in-depth multi-scale analysis of the conformations and dynamics of polar active polymers, comparing very dilute and very dense conditions. We unveil characteristic length and time scales, common to both dilute and dense systems, that recapitulate the conformational and dynamical properties of these active polymers upon varying both the polymer size and the strength of the activity. Specifically, we find that a correlation (or *looping*) length characterises the polymer conformations and the monomer dynamics. Instead, the dynamics of the center of mass can be fully characterised by the end-to-end mean-square distance and by the associated relaxation time. As such, we show that the dynamics of individual chains in melts of polar active polymers is not controlled by entanglements but only by the strength of the self-propulsion.

Active matter consists of systems whose fundamental units are able to transduce energy into persistent movement leading to features very different from the passive counterparts:[1,2]

examples abound in nature, from the macroscopic scale such as bird flocks or fish shoals,[3] down to the sub-cellular level as the cytoskeleton.[4] Of late, significant attention has focused on a specific subset of active matter – *active polymers*.[5,6] This interest arises from their biological relevance. Notable examples feature molecular motors that convert energy from chemical reactions into active motion along DNA or RNA filaments: for instance, DNA polymerase traverses DNA strands during replication, while ribosomes synthesize proteins by sliding along RNA filaments.[7] As other examples, the anomalous diffusion of chromatin loci caused by non-equilibrium processes related to enzymatic activity[8] and, at the micrometric scale, cilia and flagella used in mono- as well as multi-cellular organisms for transport and locomotion.[9] Furthermore, active polymers have been used to model the individual and collective properties of filamentous bacteria and parasites.[10–12] Interestingly, active filamentous systems have also attracted attention at the macro-scale, as worms[13] seem to provide an interesting experimental system with anomalous emerging properties.[14–17] In all cases, what makes active filaments interesting is that the energy input at the monomer level changes the typical conformation of the whole filament and influences its dynamics in a multi-scale fashion. This is true for a single filament; however, at finite density, it reverberates on the organisation of the entire system.[10,18–20] Consequently, understanding the multi-scale organisation of active polymers represents an important challenge.

In this paper we focus on polar active polymers, namely polymers where a self-propulsion force is applied to each monomer in the direction of the local backbone tangent. In this situation, significant progress has been achieved in characterizing dilute active linear and ring polymers.[21–27] Quite surprisingly, less work has been devoted to dense, entangled polymer systems (melts), feature that is relevant in many contexts, as for instance in chromatin organization.[28] In particular, the efforts were restricted to the limit of *small* activity,[29–31] with a recent exception[32] exploring the consequences of large activity for linear viscoelasticity. Here, we investigate how activity impacts on the size, shape and dynamics of entangled polymer chains in melt and compare them *vis-à-vis* with their counterparts in dilute conditions, to

highlight the main differences and the interplay between entanglements and activity.

Specifically, we employ Langevin molecular dynamics computer simulations of a well established model for polar active polymers[22] in the presence of both, Brownian thermal forces, mimicking the effect of the solvent, *and* active local tangential forces[22] of constant norm f_a imparted on every monomer, except the first and the last one, of each chain in the system. In order to express the relative strength of the activity against the thermal fluctuations, we introduce the characteristic *a*dimensional Péclet number $\mathrm{Pe} \equiv f_a\sigma/(\kappa_B T)$ where T is the temperature of the environment and κ_B is the Boltzmann constant. Here we choose $\mathrm{Pe} = 1, 5, 10, 20$, *i.e.* from low to high activity regime and, for reference, we compare these situations to the purely *passive* case $\mathrm{Pe} = 0$. We consider systems of hundreds (250, at least) polymer chains of, respectively, $N = 100, 200, 400, 800$ monomers per chain at the overall monomer density $\rho = 0.85\sigma^{-3}$ (σ is the monomer diameter) corresponding to typical melt conditions.[33] For comparison, we simulate the same chains at very dilute conditions. More details on the polymer model, systems and numerical methods used in this work are provided in Section S1 in Supporting Information (SI).

We characterize the folding of polymer chains across all scales by employing the mean-square internal distance for monomer pairs with contour length separation n,

$$\langle R^2(n)\rangle \equiv \frac{1}{N-n}\sum_{n'=1}^{N-n}\langle(\vec{r}_{n'+n}-\vec{r}_{n'})^2\rangle\,, \tag{1}$$

where $\vec{r}_n$ $(n = 1, ..., N)$ is the spatial position of monomer n and the brackets $\langle\cdot\rangle$ denote the ensemble average; we further consider the corresponding (local) scaling exponent,

$$\nu(n) \equiv \frac{1}{2}\,\frac{\log(\langle R^2(n+1)\rangle) - \log(\langle R^2(n-1)\rangle)}{\log(n+1)-\log(n-1)}\,. \tag{2}$$

For passive systems (*i.e.*, $\mathrm{Pe} = 0$), $\langle R^2(n)\rangle$ display monotonous behavior (Fig. S1(a) in SI) and the mean scaling exponents $\bar{\nu}$ obtained by averaging over the large-n behavior of $\nu(n)$ (details in Table S1 in SI) are, within the estimated uncertainties $\Delta\nu$, in good agreement

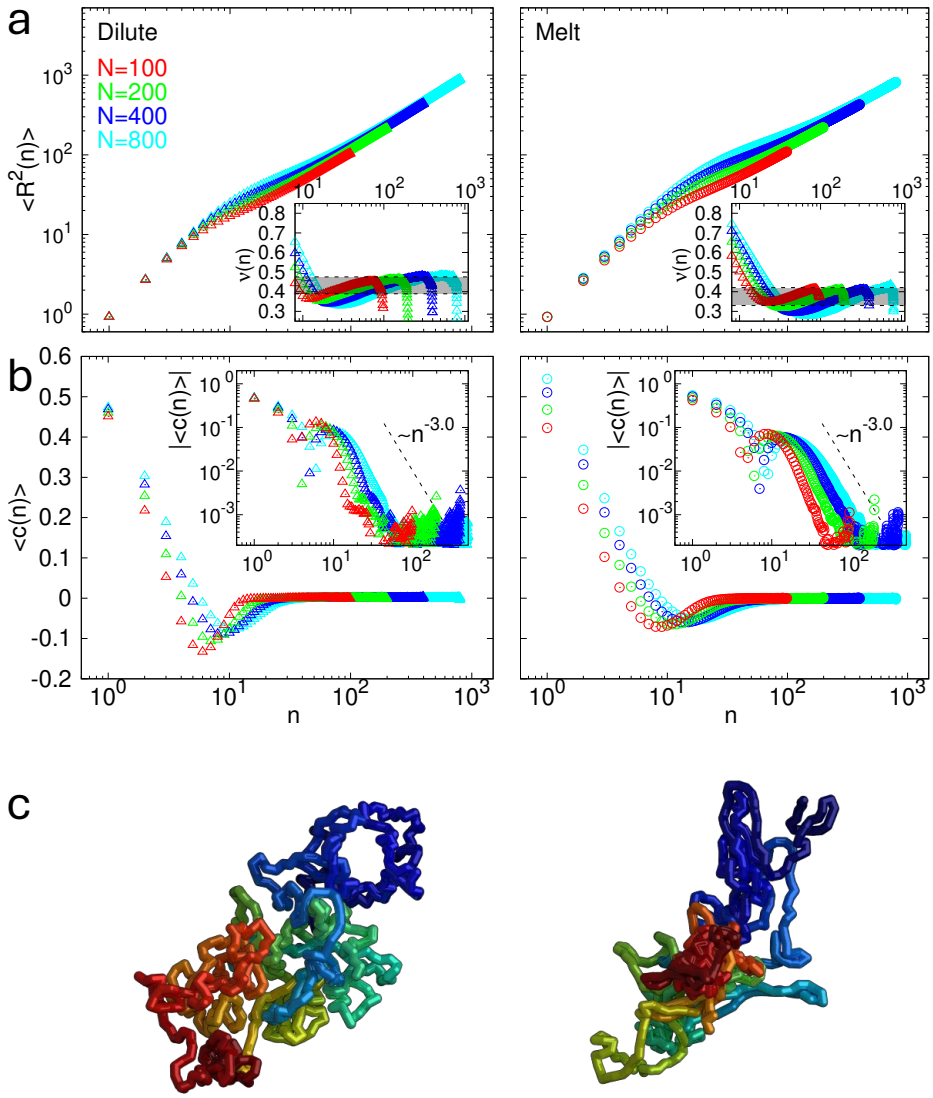

Figure 1: Single-chain properties for Pe = 20. In panels (a) and (b), symbols "△" and "○" are for dilute and melt data respectively, while different colors are for different total chain lengths N (see legend). Unless otherwise indicated, the same convention is used throughout the whole text. (a, main) Mean-square internal distance, $\langle R^2(n)\rangle$ (Eq. (1)), as a function of contour length separation, n. For passive systems and other Pe's, see Fig. S1 in SI. (a, insets) Local scaling exponent $\nu(n)$ (Eq. (2)). The shadowed strip denotes the mean scaling exponent and uncertainty $\bar{\nu}\pm\Delta\nu = 0.43\pm0.04$ (dilute) and $= 0.38\pm0.05$ (melt), see Table S1 in SI. (b, main) Bond-vector correlation function, $\langle c(n)\rangle$ (Eq. (3)), as a function of contour length separation, n, in log-lin representation. (b, insets) Corresponding norm, $|\langle c(n)\rangle|$, in log-log representation (the "$\sim n^{-3}$"-decay is for guiding the eye and purely indicative). For passive systems and other Pe's, see Fig. S2 in SI. (c) Examples of chain conformations for $N = 800$ where loops are evident. For passive systems and other Pe's, see Fig. S2 in SI.

(shadowed strips in the inset of Fig. S1(a) in SI) with established textbook[34] values $\simeq 0.6$ (dilute) and $\simeq 0.5$ (melt). On the contrary, the behavior of $\langle R^2(n)\rangle$ for active systems appears more complex (Fig. 1(a) for Pe = 20, for other Pe's see Fig. S1(b-d) in SI). At fixed Pe > 0 and N, we report three regimes for small, intermediate and large n, the latter being characterized by mean exponents $\bar{\nu}$ (shadowed strips in the insets of Fig. 1(a) and Fig. S1(b-d) in SI, see also Table S1 in SI) significantly *smaller* than those of passive systems (we will expand on this point later). At the same time, and most remarkably, for the same Pe, $\langle R^2(n)\rangle$ depends, at intermediate contour separations, also on the *total* chain length N, a feature completely absent in passive systems.

In order to rationalize this peculiar behavior, we look at the bond-vector correlation function as a function of the contour length separation n,[23,24,35]

$$\langle c(n)\rangle \equiv \frac{1}{\langle \vec{t}^2\rangle} \frac{\sum_{n'=1}^{N-1-n} \langle \vec{t}_{n'+n} \cdot \vec{t}_{n'}\rangle}{N-1-n}\,, \tag{3}$$

where $\vec{t}_n \equiv \vec{r}_{n+1} - \vec{r}_n$ ($n = 1, ..., N-1$) is the oriented bond-vector and $\langle \vec{t}^2\rangle = \sum_{n'=1}^{N-1} \langle \vec{t}_{n'}^2\rangle/(N-1)$ is the mean-square bond length, *i.e.* $c(0) = 1$ by construction. Since $\langle c(n)\rangle$ and $\langle R^2(n)\rangle$ are related to each other via the relation $\langle c(n)\rangle = \frac{1}{2}\frac{\mathrm{d}^2}{\mathrm{d}n^2}\langle R^2(n)\rangle$, features of $\langle c(n)\rangle$ may help understanding the observed phenomenon. Indeed, our results for Pe = 0 (Fig. S2(a) in SI) agree well with the known[36] power-law decays for dilute ($\langle c(n)\rangle \sim n^{-0.824}$) and melt ($\langle c(n)\rangle \sim n^{-3/2}$) conditions. On the contrary, the distinct scaling regimes displayed by $\langle R^2(n)\rangle$ for Pe > 0 are mirrored by the non-monotonous behavior of $\langle c(n)\rangle$ (Fig. 1(b) for Pe = 20, for other Pe's see Fig. S2(b-d) in SI). More precisely, for Pe > 0 $c(n)$ exhibits a distinct *negative* minimum (*i.e.*, bond-vectors become anti-correlated) at some characteristic length scale $n \equiv n_{\min}$. Afterwards, correlations decay back to zero, yet with a much steeper behavior ($\langle c(n)\rangle \sim n^{-3}$, roughly) than in passive conditions. The presence of the negative minimum, entailing the length scale $n_{\min}$, is particularly suggestive as it implies[37,38] that, both in dilute and melt conditions, active polymers tend to (double)fold into *looped* confor-

mations of loop mean contour length approximately equal to $n_{\min}$. Indeed, visual inspection of putative chain conformations for Pe = 20 (Fig. 1(c)) and for other Pe > 0 (Fig. S2(b-d) in SI) supports extensive looping, while passive counterparts appear intrinsically swollen (Fig. S2(a) in SI). This is validated further by the mean contact probability $\langle p_c(n)\rangle$ between chain monomers at contour length separation n for distinct Pe's: in particular (Fig. S3 in SI), contacts are more frequent (up to ≈ 2 orders of magnitude more in dilute chains) for $n > n_{\min}$ with respect to passive chains.[39]

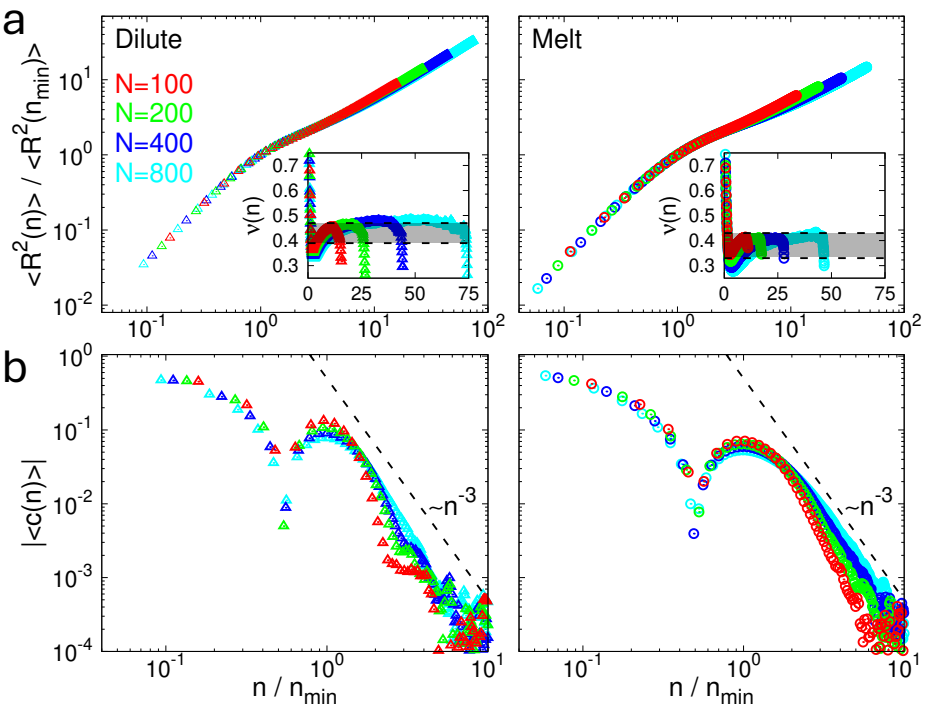

Figure 2: (a, main) Normalized mean-square internal distance, $\langle R^2(n)\rangle/\langle R^2(n_{\min})\rangle$ (Eq. (1)), as a function of normalized contour length separation, $n/n_{\min}$. (a, insets) Local scaling exponent $\nu(n)$ (Eq. (2)) as a function of $n/n_{\min}$. The shadowed strip denotes the mean scaling exponent and uncertainty $\bar{\nu} \pm \Delta\nu = 0.43 \pm 0.04$ (dilute) and $= 0.38 \pm 0.05$ (melt), see Table S1 in SI. (b) Norm of the bond-vector correlation function, $\langle c(n)\rangle$ (Eq. (3)), as a function of normalized contour length separation $n/n_{\min}$. The asymptotic $\sim n^{-3}$-decay is a guide to the eye and purely indicative. Symbols are as in Fig. 1 and Pe = 20. For passive systems and other Pe's, see Fig. S4 in SI.

Importantly, we claim that $n_{\min}$ is the *fundamental* length scale of polar active polymers. In fact, by normalizing n by $n_{\min}$ and the mean-square internal distances $\langle R^2(n)\rangle$ by $\langle R^2(n = n_{\min})\rangle$, the distinct sets of data for each Pe collapse onto one single master curve; the same

happens with the bond-correlation functions $\langle c(n)\rangle$ (Fig. 2 and Fig. S4 in SI). After rescaling, $\langle R^2(n)\rangle$ (Eq. (1)) and the associated exponent $\nu(n)$ (Eq. (2)) reveal the following noteworthy features: (i) for $n/n_{\rm min} \lesssim 1$ both dilute and melt polymers are stiffened by the activity, *i.e.* $\nu(n) > 0.5$ (insets in Fig. 2(a) and analogous panels for other Pe's in Fig. S4 in SI); (ii) for $n/n_{\rm min} \simeq 1$, the activity-induced looping of the polymer results in an unusually low value for $\nu(n)$ as the polymer tends to become locally more compact; (iii) in the long-chain limit ($n/n_{\rm min} \gtrsim 1$), for both dilute and melt polymers the mean exponents $\bar{\nu}$ are significantly smaller than those for passive chains (shadowed strips in the insets of Fig. 2(a) and Fig. S4 in SI, see Table S1 in SI for $\bar{\nu}$-values and the methodology used to extract them). We have sought further validation of polymer universal behavior for contour lengths $n > n_{\rm min}$ (and for spatial scales $> \sqrt{\langle R^2(n_{\rm min})\rangle}$) by calculating the chain form factor,[34] $S(\vec{q}) \equiv \frac{1}{N}\sum_{i,j=1}^{N}\left\langle e^{i\vec{q}\cdot(\vec{r}_i-\vec{r}_j)}\right\rangle$, as a function of the norm of the wave vector $q = |\vec{q}|$. In the scaling region $q < q_{\rm min} \equiv \frac{2\pi}{\sqrt{\langle R^2(n_{\rm min})\rangle}}$, data from different N's obey the power-law behavior[34] $S(q) \sim S(q_{\rm min})\left(\frac{q}{q_{\rm min}}\right)^{-1/\bar{\nu}}$ for *the same* mean exponents $\bar{\nu}$ of $\langle R^2(n)\rangle$ (Fig. S5 in SI).

Fig. 3 shows the scaling behaviors of $n_{\rm min}$ and $\langle R^2(n_{\rm min})\rangle$ as a function of N at fixed Pe. Interestingly, both quantities are well described by simple power-laws:

$$n_{\rm min} = n_0\left(\frac{N}{n_0}\right)^{\alpha}, \tag{4}$$

$$\langle R^2(n_{\rm min})\rangle = R_0^2\left(\frac{N}{n_0}\right)^{\beta}, \tag{5}$$

with Pe-dependent parameters n_0 and R_0 and exponents α and β[40] obtained through best fit to the data (dashed lines in Fig. 3, for values see Table S2 in SI). By Eq. (4) and Eq. (5), the chain mean-square *end-to-end* distance, $\langle R_{\rm ee}^2\rangle \equiv \langle R^2(n)\rangle|_{n=N-1}$, behaves like $\langle R_{\rm ee}^2\rangle \sim \langle R^2(n_{\rm min})\rangle(N/n_{\rm min})^{2\bar{\nu}} \sim N^{\beta+2\bar{\nu}(1-\alpha)}$. Interestingly, and no matter if in dilute or melt conditions, a direct calculation (Fig. S6 in SI) yields $\langle R_{\rm ee}^2\rangle \sim N$, implying the general relation $2\bar{\nu} = (1-\beta)/(1-\alpha)$: the comparison between this equation and the previously derived $\bar{\nu}$'s (Table S1 and S2 in SI) works relatively well. On the other hand we have not

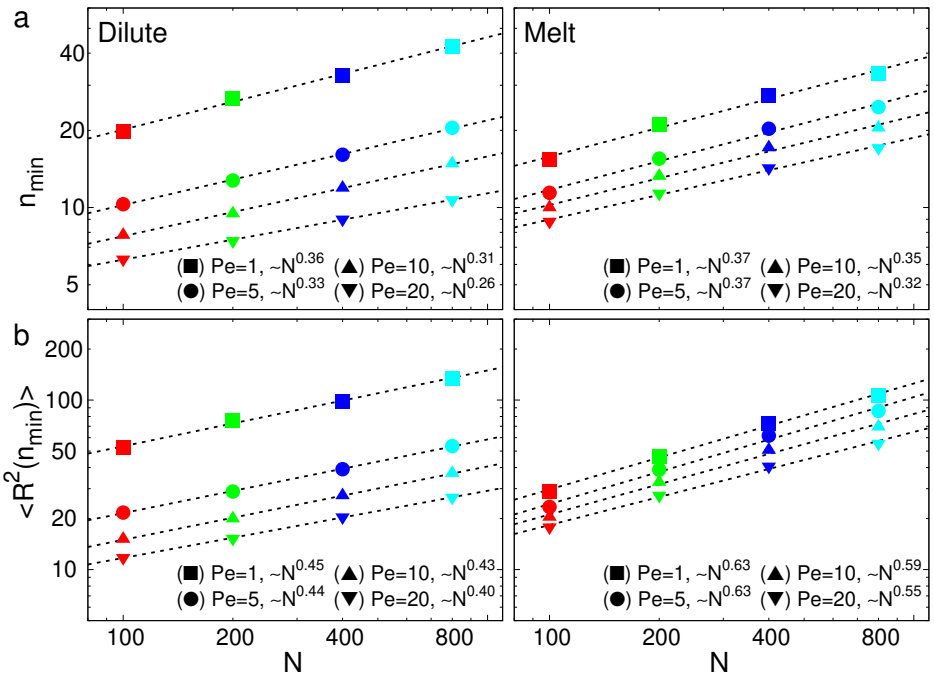

Figure 3: (a) Contour distance $n_{\min}$ (symbols) and (b) corresponding mean-square spatial distance $\langle R^2(n_{\min})\rangle$ (symbols) as a function of the polymer total length N and for Péclet number $\mathrm{Pe} > 0$. Each dashed line corresponds to the best fit of the relative data to power-laws Eq. (4) and Eq. (5), whose exponents α and β are reported in the legend (and in Table S2 in SI).

been able to find an argument to predict α and β, then we leave their derivation as a matter for future work.

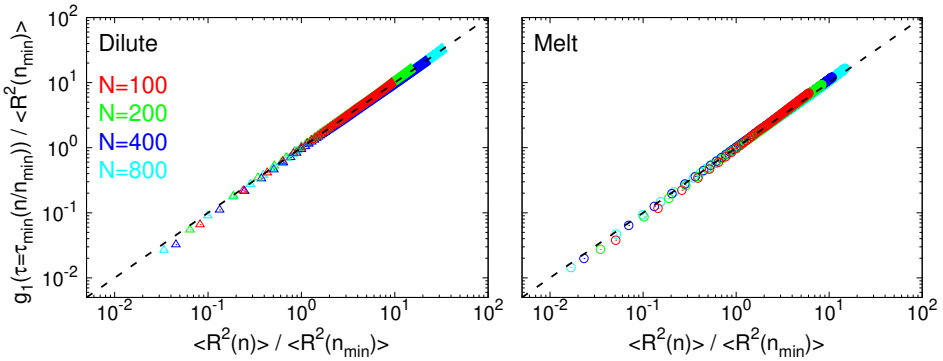

Figure 4: Parametric plots (symbols, as in Fig. 1) showing the normalized monomer mean-square displacement, $g_1(\tau)/\langle R^2(n_{\rm min})\rangle$ (Eq. (6)), calculated for $\tau = \tau_{\rm min}(n/n_{\rm min})$ as a function of the normalized mean-square internal distance, $\langle R^2(n)\rangle/\langle R^2(n_{\rm min})\rangle$ (Eq. (1)). The dashed lines correspond to $y = x$. Results are for Pe = 20, for other Pe's see Fig. S7 in SI.

We further show that $n_{\rm min}$ plays an important role in the characterization of the chain dynamics. We consider the monomer mean-square displacement,[33]

$$g_1(\tau) \equiv \frac{1}{N}\sum_{n=1}^{N}\langle(\vec{r}_n(t+\tau) - \vec{r}_n(t))^2\rangle\,, \tag{6}$$

as a function of time τ; then, we define the characteristic time scale $\tau_{\rm min}$ as $g_1(\tau_{\rm min}) = \langle R^2(n_{\rm min})\rangle$. Interestingly, data follow the notable relation $g_1(\tau = \tau_{\rm min}(n/n_{\rm min})) \simeq \langle R^2(n)\rangle$ (Fig. 4 for Pe = 20 and Fig. S7(a-c) in SI), namely monomers, on average, move *along* the contour length of their own chain. Conversely, passive systems (Fig. S7(d) in SI) do not display such behavior. Overall, activity triggers a kind of motion where each monomer is, on average, pulled along the polymer local shape before the chain reorganizes into a new conformation.

Finally, the material properties of the system, such as its viscosity, are of crucial interest for polymer melts and can be connected to the dynamics of the center of mass of the chains.[34] We thus investigate $g_3(\tau)$, the mean-square displacement of the chain centre of mass $\vec{r}_{\rm CM}(t) \equiv$

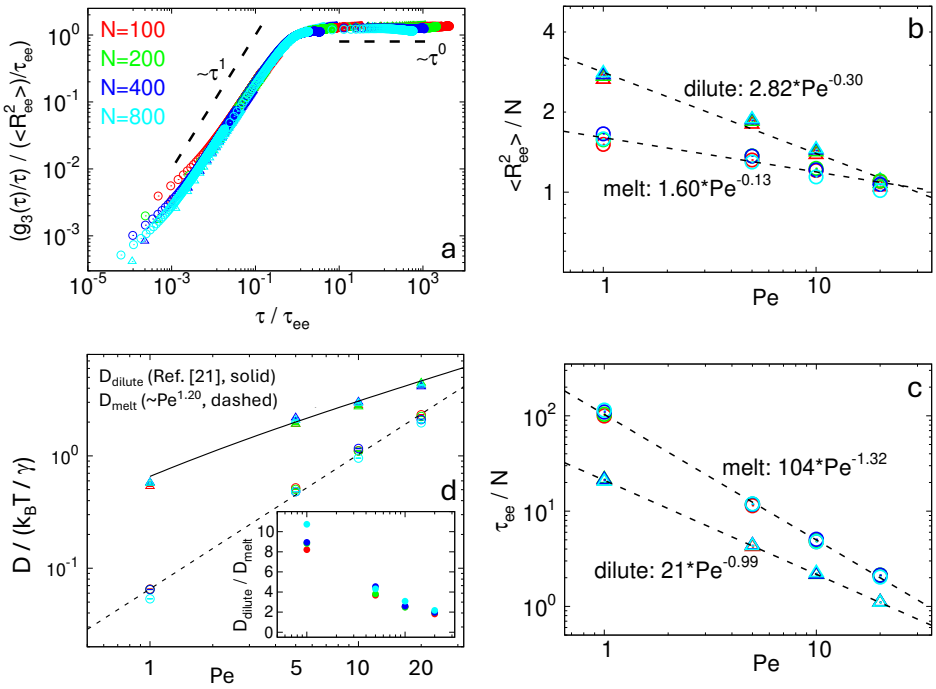

Figure 5: (a) Mean-square displacement of the chain centre of mass per unit time, $g_3(\tau)/\tau$ (Eq. (7)), normalized by $\langle R_{\rm ee}^2\rangle/\tau_{\rm ee}$ as a function of normalized time $\tau/\tau_{\rm ee}$ at Pe = 20. For other Pe's, see Fig. S8 in SI. (b) Chain mean-square end-to-end distance $\langle R_{\rm ee}^2\rangle$ normalized by N as a function of Pe (symbols) and corresponding power-law best fits (lines). (c) Chain relaxation time $\tau_{\rm ee}$ normalized by N as a function of Pe (symbols) and corresponding power-law best fits (lines). (d, main) Long-time diffusion coefficient of the centre of mass, D (in units of monomer diffusion coefficient, see Sec. S1B in SI), as a function of Pe. Lines recapitulating the data correspond to the analytical expression for dilute chains proposed in[22] and a phenomenological power-law fit ($\sim$ Pe$^{1.20}$) for melts. In panels from (a) to (d, main), symbols are as in Fig. 1. (d, inset) Corresponding ratios, $D_{\rm dilute}/D_{\rm melt}$, between diffusion coefficients in dilute and melt conditions as a function of Pe.

$\frac{1}{N}\sum_{n=1}^{N}\vec{r}_n(t)$, defined as

$$g_3(\tau) \equiv \langle(\vec{r}_{\rm CM}(t+\tau) - \vec{r}_{\rm CM}(t))^2\rangle\,, \tag{7}$$

as a function of time τ. Previous works[22,25,35,41] on dilute polar active polymers have shown that, with respect to passive systems, $g_3(\tau)$ displays a ballistic regime up to the chain relaxation time $\tau_{\rm ee}$, defined by the relation $g_3(\tau_{\rm ee}) = \langle R^2_{\rm ee}\rangle$. At times $\tau > \tau_{\rm ee}$, an active diffusive regime ensues $g_3(\tau) = 6D\tau$, where the active diffusion coefficient D *increases* with Pe and is *independent* of the chain contour length N, in contrast with the passive, hydrodynamic-free, predictions.[34] We show here that such features are present also in melt conditions. To start, we report that, upon normalizing $g_3(\tau)$ by the corresponding $\langle R^2_{\rm ee}\rangle$ and τ by $\tau_{\rm ee}$, data from systems at different values of N and Pe strikingly collapse onto the same universal curve that is valid for both dilute and melt systems in the ballistic and active diffusive regime (Fig. 5(a) and Fig. S8 in SI). This result is quite remarkable for polymer melts as, according to the classical tube model,[34] for $\tau < \tau_{\rm ee}$ single-chain dynamics is expected to be sub-diffusive, $g_3 \sim t^{1/2}$, since motion is confined in a tube-like region resulting from the *topological* constraints (*entanglements*) imposed by the surrounding chains. The absence of this regime in melt conditions suggests that polymer dynamics is controlled by activity, that governs both $\langle R^2_{\rm ee}\rangle$ and $\tau_{\rm ee}$; entanglements do affect the overall chain mobility only at small values of Pe, at least within the values of N considered in this work. In support of this point, we report the following peculiar scaling of $\langle R^2_{\rm ee}\rangle$ (complementing the results of Fig. S6 in SI) and of $\tau_{\rm ee}$ in melt conditions: $\langle R^2_{\rm ee}\rangle \propto N/{\rm Pe}^{0.1}$ (Fig. 5(b)) and $\tau_{\rm ee} \propto N/{\rm Pe}^{1.3}$ (Fig. 5(c)). Notice, in particular, the differences with the infinite dilution case, where $\langle R^2_{\rm ee}\rangle \sim N/{\rm Pe}^{0.3}$ and $\tau_{\rm ee} \propto N/{\rm Pe}$, and with passive melts, where[34] $\tau_{\rm ee} \sim N^3$. As $D \propto \langle R^2_{\rm ee}\rangle/\tau_{\rm ee}$, we indeed recover the scaling of D as function of N and Pe for melts, $D \propto N^0 \cdot {\rm Pe}^{1.2}$ (dashed line in Fig. 5(d)). While results for dilute chains are in agreement with the analytical predictions[22] (solid line in Fig. 5(d), see also the brief recapitulation in Sec. S2A in SI), notice that D

has a steeper increase in melt; as such, although dilute chains diffuse systematically faster than in melt, the gap between the two appears to be narrowing for growing Pe (see inset in Fig. 5(d)) until the two set-up's become substantially equivalent at sufficiently high values of Pe. These findings align with the reported observations that the relaxation times τ_{ee} for the two set-up's become increasingly close to each other as Pe increases (Fig. 5(c)).

To summarize, in this work we have investigated the impact of activity on the conformational and dynamical properties of linear chains in melt conditions as compared to dilute counterparts. The multi-scale analysis of the conformations highlighted a fundamental contour length scale, n_{min}, which governs both the conformations of the active chains as well the dynamics of the individual monomers. n_{min} allows us to identify master curves for the mean-square internal distances ($\langle R^2(n)\rangle$, Fig. 2 and Fig. S4 in SI) and the single-chain form factors ($S(q)$, Fig. S5 in SI); the rescaling at large contour separations emerges more clearly in Fourier space, possibly due to the limited statistics available for $\langle R^2(n)\rangle$. Notably, we report systematic deviations from the statistics of passive chains in both dilute and melt conditions, ascribable to the formation of loops within the chains (see conformations in Fig. 1(c) and Figs. S2 in SI) for contour lengths $n > n_{\mathrm{min}}$. In particular, beyond n_{min} the mean scaling exponents $\bar{\nu}$ extracted from $\langle R^2(n)\rangle$ *decrease* significantly (by 20-25%) with Pe (Table S1 in SI), from values $\bar{\nu} = 0.54 \pm 0.06$ (dilute) and $\bar{\nu} = 0.51 \pm 0.04$ (melt) for $\mathrm{Pe} = 0$ to $\bar{\nu} = 0.43 \pm 0.04$ (dilute) and $\bar{\nu} = 0.38 \pm 0.05$ (melt) for our highest $\mathrm{Pe} = 20$. The scaling of $\langle R^2(n)\rangle$ governed by $\bar{\nu}$, in combination with the two observed scalings $n_{\mathrm{min}} \sim N^{\alpha}$ and $\langle R^2(n_{\mathrm{min}})\rangle \sim N^{\beta}$ (Fig. 3), accounts for the observed scaling of the mean-square *end-to-end* distance $\langle R^2_{\mathrm{ee}}\rangle \sim N$ (Fig. S6 in SI) that holds for *both* dilute[32] and melt conditions. In turn, this suggests that active chains do not remain completely *self-similar*[42] (as also pointed out by the mean-square internal distance $\langle R^2(n)\rangle$, see Fig. 1(a) and Fig. S1 in SI). This is in marked contrast with traditional[34] passive chains, whose self-similarity is well reflected here by the agreement between the corresponding $\bar{\nu}$ and the scaling of $\langle R^2_{\mathrm{ee}}\rangle$ (Fig. S6 and Table S1 in SI). Furthermore, although polar active chains may exhibit a non-homogeneous collapse

along its profile,[43] our analysis, averaging along the contour, unveils a property that should be robust against such inhomogeneity.

At the same time, we have shown that the observed scaling $\langle R_{\rm ee}^2 \rangle \sim N$ plays a role in the characterization of chain dynamics. First, due to tangential propulsion, monomers perform "railway motion" along the contour path of the backbone. We further find that, remarkably, both dilute and melt systems exhibit the same centre of mass dynamics (Fig. 5(a)) governed by the length scale $\langle R_{\rm ee}^2 \rangle$ and by the time scale $\tau_{\rm ee}$. At long times, $\tau \gg \tau_{\rm ee}$, both systems diffuse with a diffusion coefficient, D, which increases with Pe (Fig. 5(d)) and is independent on N. However, as mentioned, D has a stronger dependence on Pe in melts, possibly hinting at the emergence of multi-chain effects that go beyond the railway motion.

Taken together, our results suggest that both chain conformations and dynamics present universal features that are independent of whether chains are dilute or in melt. In melt, in particular, the well known[34] slowing-down in passive systems due to entanglements become negligible when chains are subjected to tangential active forces. Interestingly, this recapitulates theoretical results[29] for a slow-reptating chain showing that tangential drifts (no matter how weak) can easily overwhelm reptation and, then, enhance chain's diffusivity. At the same time, our results align with experimental observations[15] on active worms reporting a decrease in system viscosity with activity and a milder dependence on concentration compared to passive entangled systems. Moreover, as recently shown,[32] for polar propelled entangled chains the plateau modulus, G_0, that encodes the elastic response of the system,[34] depends on the active forces in the systems and is not anymore simply proportional[34] to the mean concentration of entanglement lengths as in passive conditions.

We conclude with a perspective for future work. Since active polymers are deeply out-of-equilibrium, the emerging properties of these systems may depend crucially on the details of the model: other models of active polymers and, further, other implementations for active tangential forces can be defined. In the case of non-constant polar forces,[44] interesting viscoelastic properties have been already displayed;[32] it would be then interesting to confirm

the role of $n_{\min}$ also in this setting. Further, the so-called "two-temperature" model[18] displays peculiar entanglement properties for rings[45] as well as for linear polymers.[46] Furthermore, to the best of our knowledge, no research has been done on the entanglement of active Brownian polymers[6] or active Rouse chains, *i.e.* chains driven by athermal noise correlated along the backbone[47]. So, it would be interesting to see whether the ideas discussed in the present work apply to other models and, in general, what are the defining features of each one of these "minimal" models of active polymer. This would lay important groundwork for the application of these models in more complex settings.

Supporting Information

Complementary details on: polymer model, molecular dynamics computer simulations and preparation and equilibration of polymer configurations, single-chain diffusion and mean-square end-to-end distance. Additional figures on: polymer structure (internal and end-to-end distances, bond-vector correlations with visualization of chain conformations, contact probabilities, single-chain form factor), polymer dynamics (mean-square displacements for monomers and chain centre of mass). Supporting tables for: mean values of scaling exponent ν ($\bar{\nu}$), scaling parameters $n_{\min}$ and $\langle R^2(n_{\min})\rangle$.

Acknowledgement

This work was supported by a STSM Grant from COST Action CA17139 (eutopia.unitn.eu) funded by COST (www.cost.eu). E.L. acknowledges support from the MIUR grant Rita Levi Montalcini. A.R. acknowledges financial support from PNRR Grant CN_00000013_CN-HPC, M4C2I1.4, spoke 7, funded by Next Generation EU.

References

(1) Ramaswamy, S. The mechanics and statistics of active matter. *Annu. Rev. Condens. Matter Phys.* **2010**, *1*, 323–345.

(2) Marchetti, M. C.; Joanny, J.-F.; Ramaswamy, S.; Liverpool, T. B.; Prost, J.; Rao, M.; Simha, R. A. Hydrodynamics of soft active matter. *Rev. Mod. Phys.* **2013**, *85*, 1143.

(3) Vicsek, T.; Zafeiris, A. Collective motion. *Phys. Rep.* **2012**, *517*, 71–140.

(4) Fletcher, D. A.; Mullins, R. D. Cell mechanics and the cytoskeleton. *Nature* **2010**, *463*, 485–492.

(5) Winkler, R. G.; Elgeti, J.; Gompper, G. Active polymers - Emergent conformational and dynamical properties: A brief review. *J. Phys. Soc. Jpn* **2017**, *86*, 101014.

(6) Winkler, R. G.; Gompper, G. The physics of active polymers and filaments. *J. Chem. Phys.* **2020**, *153*, 040901.

(7) Alberts, B.; Johnson, A.; Lewis, J.; Raff, M.; Roberts, K.; Walter, P. *Molecular Biology of the Cell. 4th edition*; Garland science, 2002.

(8) Weber, S. C.; Spakowitz, A. J.; Theriot, J. A. Nonthermal ATP-dependent fluctuations contribute to the in vivo motion of chromosomal loci. *Proc. Natl. Acad. Sci. USA* **2012**, *109*, 7338–7343.

(9) Gilpin, W.; Bull, M. S.; Prakash, M. The multiscale physics of cilia and flagella. *Nature Reviews Physics* **2020**, *2*, 74–88.

(10) Patra, P.; Beyer, K.; Jaiswal, A.; Battista, A.; Rohr, K.; Frischknecht, F.; Schwarz, U. S. Collective migration reveals mechanical flexibility of malaria parasites. *Nature Physics* **2022**, *18*, 586–594.

(11) Faluweki, M. K.; Cammann, J.; Mazza, M. G.; Goehring, L. Active spaghetti: collective organization in cyanobacteria. *Physical Review Letters* **2023**, *131*, 158303.

(12) Kurjahn, M.; Abbaspour, L.; Papenfuß, F.; Bittihn, P.; Golestanian, R.; Mahault, B.; Karpitschka, S. Collective self-caging of active filaments in virtual confinement. *arXiv preprint arXiv:2403.03093* **2024**,

(13) Deblais, A.; Prathyusha, K.; Sinaasappel, R.; Tuazon, H.; Tiwari, I.; Patil, V. P.; Bhamla, M. S. Worm blobs as entangled living polymers: from topological active matter to flexible soft robot collectives. *Soft Matter* **2023**, *19*, 7057–7069.

(14) Deblais, A.; Maggs, A.; Bonn, D.; Woutersen, S. Phase separation by entanglement of active polymerlike worms. *Phys. Rev. Lett.* **2020**, *124*, 208006.

(15) Deblais, A.; Woutersen, S.; Bonn, D. Rheology of entangled active polymer-like T. tubifex worms. *Phys. Rev. Lett.* **2020**, *124*, 188002.

(16) Ozkan-Aydin, Y.; Goldman, D. I.; Bhamla, M. S. Collective dynamics in entangled worm and robot blobs. *Proc. Natl. Acad. Sci. USA* **2021**, *118*, e2010542118.

(17) Patil, V. P.; Tuazon, H.; Kaufman, E.; Chakrabortty, T.; Qin, D.; Dunkel, J.; Bhamla, M. S. Ultrafast reversible self-assembly of living tangled matter. *Science* **2023**, *380*, 392–398.

(18) Smrek, J.; Chubak, I.; Likos, C. N.; Kremer, K. Active topological glass. *Nature Communications* **2020**, *11*, 26.

(19) Dunajova, Z.; Mateu, B. P.; Radler, P.; Lim, K.; Brandis, D.; Velicky, P.; Danzl, J. G.; Wong, R. W.; Elgeti, J.; Hannezo, E., et al. Chiral and nematic phases of flexible active filaments. *Nature Physics* **2023**, *19*, 1916–1926.

(20) Miranda, J. P.; Locatelli, E.; Valeriani, C. Self-Organized States from Solutions of

Active Ring Polymers in Bulk and under Confinement. *Journal of Chemical Theory and Computation* **2024**, *20*, 1636–1645, DOI: 10.1021/acs.jctc.3c00818.

(21) Isele-Holder, R. E.; Elgeti, J.; Gompper, G. Self-propelled worm-like filaments: spontaneous spiral formation, structure, and dynamics. *Soft Matter* **2015**, *11*, 7181–7190.

(22) Bianco, V.; Locatelli, E.; Malgaretti, P. Globulelike conformation and enhanced diffusion of active polymers. *Phys. Rev. Lett.* **2018**, *121*, 217802.

(23) Locatelli, E.; Bianco, V.; Malgaretti, P. Activity-induced collapse and arrest of active polymer rings. *Phys. Rev. Lett.* **2021**, *126*, 097801.

(24) Foglino, M.; Locatelli, E.; Brackley, C.; Michieletto, D.; Likos, C.; Marenduzzo, D. Non-equilibrium effects of molecular motors on polymers. *Soft Matter* **2019**, *15*, 5995–6005.

(25) Philipps, C. A.; Gompper, G.; Winkler, R. G. Tangentially driven active polar linear polymers—An analytical study. *J. Chem. Phys.* **2022**, *157*, 194904.

(26) Philipps, C. A.; Gompper, G.; Winkler, R. G. Dynamics of active polar ring polymers. *Phys. Rev. E* **2022**, *105*, L062501.

(27) Vatin, M.; Kundu, S.; Locatelli, E. Conformation and dynamics of partially active linear polymers. *Soft Matter* **2024**, *20*, 1892–1904.

(28) Rosa, A.; Everaers, R. Structure and Dynamics of Interphase Chromosomes. *Plos Comput. Biol.* **2008**, *4*, e1000153.

(29) Tejedor, A. R.; Ramiírez, J. Reptation of active entangled polymers. *Macromolecules* **2019**, *52*, 8788–8792.

(30) Tejedor, A. R.; Ramírez, J. Dynamics of entangled polymers subjected to reptation and drift. *Soft Matter* **2020**, *16*, 3154–3168.

(31) Tejedor, A. R.; Carracedo, R.; Ramírez, J. Molecular dynamics simulations of active entangled polymers reptating through a passive mesh. *Polymer* **2023**, *268*, 125677.

(32) Breoni, D.; Kurzthaler, C.; Liebchen, B.; Löwen, H.; Mandal, S. Giant Activity-Induced Stress Plateau in Entangled Polymer Solutions. *arXiv:2310.02929v1* **2023**,

(33) Kremer, K.; Grest, G. S. Dynamics of entangled linear polymer melts: A molecular-dynamics simulation. *J. Chem. Phys.* **1990**, *92*, 5057–5086.

(34) Rubinstein, M.; Colby, R. H. *Polymer Physics*; Oxford University Press: New York, 2003.

(35) Fazelzadeh, M.; Irani, E.; Mokhtari, Z.; Jabbari-Farouji, S. Effects of inertia on conformation and dynamics of tangentially driven active filaments. *Phys. Rev. E* **2023**, *108*, 024606.

(36) Wittmer, J. P.; Meyer, H.; Baschnagel, J.; Johner, A.; Obukhov, S.; Mattioni, L.; Müller, M.; Semenov, A. N. Long Range Bond-Bond Correlations in Dense Polymer Solutions. *Phys. Rev. Lett.* **2004**, *93*, 147801.

(37) Müller, M.; Wittmer, J. P.; Cates, M. E. Topological effects in ring polymers. II. Influence of persistence length. *Phys. Rev. E* **2000**, *61*, 4078–4089.

(38) Rosa, A.; Everaers, R. Ring Polymers in the Melt State: The Physics of Crumpling. *Phys. Rev. Lett.* **2014**, *112*, 118302.

(39) Notice that here we study static loops properties, and we do not ask instead on the typical time scales for loops formation. This interesting point, also connected to classical mean-first passage time theories in polymer systems (*e.g.*, Ghosh and Spakowitz, "Active and thermal fluctuations in multi-scale polymer structure and dynamics", Soft Matter 2022, 18, 6629-6637), goes beyond the scopes of the paper and it will be matter for future investigations.

(40) Notice that Eq. (4) and Eq. (5) imply that $\langle R^2(n_{\min})\rangle \sim n_{\min}^{\beta/\alpha}$, with typical values $\beta/\alpha > 1$ (Table S1 in SI) in agreement with fiber stiffening at short contour length scales.

(41) Li, J.-X.; Wu, S.; Hao, L.-L.; Lei, Q.-L.; Ma, Y.-Q. Nonequilibrium structural and dynamic behaviors of polar active polymer controlled by head activity. *Physical Review Research* **2023**, *5*, 043064.

(42) A situation echoing this condition is for globular polymers of total contour length N in bad solvent conditions.[34] Here, the end-to-end distance of the polymer scales as $R_{\text{ee}} \sim N^{1/3}$. On the other hand, on length scales $< R_{\text{ee}}$, the local structure of the system is no different than the one of an ordinary polymer melt, *i.e.* $\langle R(n)\rangle \sim n^{1/2}$.

(43) Tejedor, A. R.; Ramírez, J.; Ripoll, M. Progressive polymer deformation induced by polar activity and the influence of inertia. *Physical Review Research* **2024**, *6*, L032002.

(44) Anand, S. K.; Singh, S. P. Structure and dynamics of a self-propelled semiflexible filament. *Phys. Rev. E* **2018**, *98*, 042501.

(45) Micheletti, C.; Chubak, I.; Orlandini, E.; Smrek, J. Topology-Based Detection and Tracking of Deadlocks Reveal Aging of Active Ring Melts. *ACS Macro Letters* **2024**, *13*, 124–129.

(46) Li, J.; Zhang, B.; Wang, Z.-Y. Activity-induced stiffness, entanglement network and dynamic slowdown in unentangled semidilute polymer solutions. *Soft Matter* **2024**, *20*, 5174–5182.

(47) Osmanović, D.; Rabin, Y. Dynamics of active Rouse chains. *Soft matter* **2017**, *13*, 963–968.

TOC Graphic

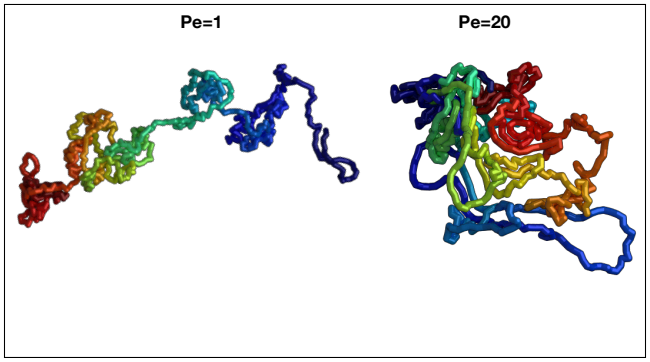

– Supporting Information –
Universal time and length scales of polar active polymer melts

Mattia Alberto Ubertini*
Scuola Internazionale Superiore di Studi Avanzati (SISSA), Via Bonomea 265, 34136 Trieste, Italy

Emanuele Locatelli†
Department of Physics and Astronomy, University of Padova, Via Marzolo 8, I-35131 Padova, Italy and INFN, Sezione di Padova, Via Marzolo 8, I-35131 Padova, Italy

Angelo Rosa‡
Scuola Internazionale Superiore di Studi Avanzati (SISSA), Via Bonomea 265, 34136 Trieste, Italy

CONTENTS

* mubertin@sissa.it; Current affiliation: Friedrich Miescher Institute for Biomedical Research (FMI), 4056 Basel, Switzerland
† emanuele.locatelli@unipd.it
‡ Corresponding author: anrosa@sissa.it

In this Supporting Information file, we provide more specific details on the polymer model used (Sec. S1 A), on the compositions of the considered polymer systems and technical details on the molecular dynamics computer simulations (Sec. S1 B) and on the initial preparation and following equilibration of the systems (Sec. S1 C). We conclude, with a short recap (Sec. S2 A) of the theory for active polymer model diffusion first discussed in Refs. [1, 2] and used in the main text, and a brief overview on the scaling properties of the mean-square end-to-end distance for our polymers (Sec. S2 B).

S1. POLYMER MODEL AND METHODS

A. Numerical model for polar active polymers

Chain connectivity and monomer-monomer interactions for dilute and melt linear chains are accounted for by a suitably modified version of the classical polymer model by Kremer and Grest [3]. Specifically, excluded volume interactions between beads (including consecutive ones along the contour length of the chains) are described in terms of the shifted and truncated Lennard-Jones (LJ) potential:

$$U_{\rm LJ}(r) = \begin{cases} 4\epsilon \left[\left(\frac{\sigma}{r}\right)^{12} - \left(\frac{\sigma}{r}\right)^{6} + \frac{1}{4} \right] & r \leq 2^{1/6}\sigma \\ 0 & r > 2^{1/6}\sigma \end{cases} , \tag{S1}$$

where r denotes the spatial separation between the bead centers. By denoting with κ_B the Boltzmann constant, the energy scale is set to $\epsilon = 20\,\kappa_B T$ (against the standard $\epsilon = 1\,\kappa_B T$ [3]) where T and σ are, respectively, the units of temperature and length in our simulation. The unit of energy is thus taken as the thermal energy, *i.e.* $\kappa_B T = 1$. Further, nearest-neighbour monomers along the contour of the chains are connected by the finitely extensible nonlinear elastic (FENE) potential, given by:

$$U_{\rm FENE}(r) = \begin{cases} -0.5 k R_0^2 \ln\left(1 - (r/R_0)^2\right) & r \leq R_0 \\ \infty & r > R_0 \end{cases} , \tag{S2}$$

where $k = 30\epsilon/\sigma^2 = 600\,\kappa_B T/\sigma^2$ is the spring constant and $R_0 = 1.5\sigma$ is the maximum extension of the elastic FENE bond [4]. Finally, polymer activity is taken into account by imposing that the i-th monomer of each chain of spatial coordinates $\vec{r}_i$ (for $i = 2, ..., N-1$, with N being the total number of monomers of the chain) is subject to the active force $\vec{F}_i$ [1]:

$$\vec{F}_i = f_a \frac{\vec{r}_{i+1} - \vec{r}_{i-1}}{|\vec{r}_{i+1} - \vec{r}_{i-1}|} , \tag{S3}$$

of constant magnitude f_a and instantaneous orientation directed along the tangent to the polymer chain at $\vec{r}_i$. Notice that the first and the last monomers of each chain are (conventionally, see [1]) excluded by the active perturbation because those monomers have only one, instead of two, neighbor along the chain. As described in the main text, the relative importance of the active forces *vs.* the thermal ones is quantified in term of the so called Péclet number Pe, defined as

$$\mathrm{Pe} \equiv \frac{f_a \sigma}{\kappa_B T} , \tag{S4}$$

We consider values $\mathrm{Pe} = 1, 5, 10, 20$ and, for comparison, the purely passive case $\mathrm{Pe} = 0$.

B. Simulation details

We consider monodisperse melts of M linear polymer chains, each chain being made of N monomers. Specifically, we consider systems with compositions $(M, N) = (1000, 100)$, $(500, 200)$ and $(250, 400)$ (*i.e.*, $M \times N = 100{,}000$ monomers in total) and $(M, N) = (250, 800)$ (*i.e.*, $M \times N = 200{,}000$ monomers in total). As in the original work by Kremer and Grest [3], we maintain a fixed monomer density of $\rho = 0.85\sigma^{-3}$ for all polymer compositions.

As mentioned in the main text, we compare simulation results for active polymer melts to those for single self-avoiding active polymers in dilute conditions. In the latter case we simulate the same systems as the ones of the

set-up's described above, with deactivated *inter*-chain LJ (see Eq. (S1)) excluded volume interactions. This allows us to effectively simulate replicas of linear chains in dilute conditions.

The static and kinetic properties of chains are studied using fixed-volume and constant-temperature *molecular dynamics* (MD) simulations with implicit solvent and periodic boundary conditions. MD simulations are performed by using the LAMMPS package [5]. By introducing the MD time-unit $\tau_{\rm MD} = \sigma\sqrt{m/\kappa_B T}$, we integrate the equations of motion by using the velocity-Verlet algorithm. We set Δt, the integration time step of the algorithm, as the following: (i) $\Delta t = 0.01\,\tau_{\rm MD}$ for passive polymers (*i.e.*, Pe = 0) and (ii) $\Delta t = 0.001\,\tau_{\rm MD}$ for active systems with Pe > 0 (in order to prevent accidental strand-crossings, especially in the regime of high active forces). Finally, in order to ensure the overdamped regime [2], the friction coefficient γ is $= 20\,\tau_{MD}^{-1}$.

C. Preparation of initial chain configurations and check for equilibration

Preparation of melts of linear chains poses no particular technical problem. Chains up to $N = 400$ were initially arranged inside the simulation box and the system is passively (*i.e.*, active forces at this stage are turned off) let towards complete equilibration (defined as after the chains have drifted from their original positions for several times their own root-mean-square end-to-end distance, $\sqrt{\langle R_{\rm ee}^2\rangle}$ (where $\langle R_{\rm ee}^2\rangle$ is Eq. (1) in the main text with $n = N-1$). For the case with $N = 800$ this procedure becomes tediously long, so we have prepared first the system on the FCC lattice and, then, let it partially equilibrate by means of the efficient kinetic Monte Carlo algorithm used in [6, 7]. After completing this step, we move the whole system back off-lattice again and let it evolve by standard MD: being the system highly entangled for the polymer contour length considered, we performed one last equilibration check by verifying that the main structural properties of the chains are effectively independent of the initial preparation [8].

Following this initial set-up, the polymer conformations become the starting point for the production runs of systems in the presence of active force (*i.e.*, for Pe > 0) and, also, for their passive counterparts (Pe = 0). The typical production run consists of $10^6\,\tau_{\rm MD}$-units.

S2. MORE ON SINGLE-CHAIN PROPERTIES

A. Long-time diffusion coefficient

The long time diffusion coefficient of isolated polar active polymers can be computed analytically [1, 2]. We start from the diffusion coefficient for an Active Brownian Particle,

$$D = D_t + \frac{\tau_r\, v_a^2}{2d} = D_t + \frac{\tau_r\,(F_a/\gamma)^2}{2d}\,, \tag{S5}$$

where $v_a = f_a/\gamma$ is the self-propulsion velocity and $D_t = \kappa_B T/\gamma$; d is the dimensionality of the system (here, $d = 3$). For a polar active polymer: (i) $\gamma = N\gamma_0$, γ_0 being the friction coefficient of a single monomer; (ii) $F_a = f_a R_{\rm ee}/\sigma$, with $f_a = \frac{\kappa_B T}{\sigma}$Pe as in Eq. (S4), $R_{\rm ee}$ being the (root mean-square) end-to-end distance and σ the mean bond length (Sec. S1 A); (iii) $\tau_r = \tau_{\rm ee}$ corresponds to the chain relaxation time (defined in the main text). If f_a is sufficiently large, we can disregard the passive contribution and write

$$D = \frac{\tau_{\rm ee}}{2d}\left(\frac{\rm Pe}{N}\frac{\kappa_B T}{\gamma_0}\frac{R_{\rm ee}}{\sigma}\right)^2 = \frac{1}{2d}\frac{\tau_{\rm ee} D_0}{\sigma^2}\frac{\rm Pe^2}{N^2}\frac{R_{\rm ee}^2}{\sigma^2}D_0\,. \tag{S6}$$

We now consider what is reported in Fig. 5(a) in the main text and Fig. S8 here, *i.e.* $(g_3(\tau)/\tau)/(R_{\rm ee}^2/\tau_{\rm ee})$. We focus on the long time diffusion: we have by definition that $g_3(\tau) = 2dD\tau$, from which $g_3(\tau)/\tau = 2dD$. As such, the data reported in Fig. 5(a) in the main text and Fig. S8 here show that

$$(g_3(\tau)/\tau)/(R_{\rm ee}^2/\tau_{\rm ee}) = (2dD)/(R_{\rm ee}^2/\tau_{\rm ee}) \simeq 1.5\,. \tag{S7}$$

From Eq. (S6) we get

$$\frac{2dD}{R_{\rm ee}^2/\tau_{\rm ee}} = \left(\frac{\tau_{\rm ee}D_0}{\sigma^2}\right)^2\frac{\rm Pe^2}{N^2} = \left(\tau_0\frac{N}{\rm Pe}\right)^2\frac{\rm Pe^2}{N^2} = \tau_0^2\,, \tag{S8}$$

where D_0 is the passive diffusion coefficient of a single monomer and we have used the relation $\tau_{\rm ee}D_0/\sigma^2 = \tau_0 N/{\rm Pe}$, shown to be valid in dilute conditions for the characteristic relaxation time $\tau_{\rm ee}$ in Fig. 5(c) of the main text. As $D_0 = \kappa_B T/\gamma = 0.05$ in this work, from Fig. 5(c) we get $\tau_0 = 1.05$. As such, the analytical prediction is $(2dD)/(R_{\rm ee}^2/\tau_{\rm ee}) = 1.1$.

B. Mean-square end-to-end distance

Results for $\langle R_{\mathrm{ee}}^2 \rangle$ are reported in Fig. S6. The passive case (Pe = 0) behaves as expected, dilute linear chains exhibit swelling compared to chains within the melt, with their sizes scaling differently. Specifically, the scaling exponent for dilute chains is $\nu = 0.588$ [9], while in the melt, linear chains follow random walk statistics [9] and their sizes scale with $\nu = 0.5$. Notably, in both systems, as Pe grows, the polymers crumple, a feature already seen for dilute active linear chains [1]. Remarkably, at high Péclet number $\simeq 10/20$, across all considered polymer lengths N, $\langle R_{\mathrm{ee}}^2 \rangle$ for both dilute and melt cases converge to similar values. Moreover, always at high activity, the scaling of $\langle R_{\mathrm{ee}}^2 \rangle$ appears to align with ideal behavior, exhibiting a scaling exponent of $\nu = 0.5$ for both cases.

SUPPORTING FIGURES & TABLES

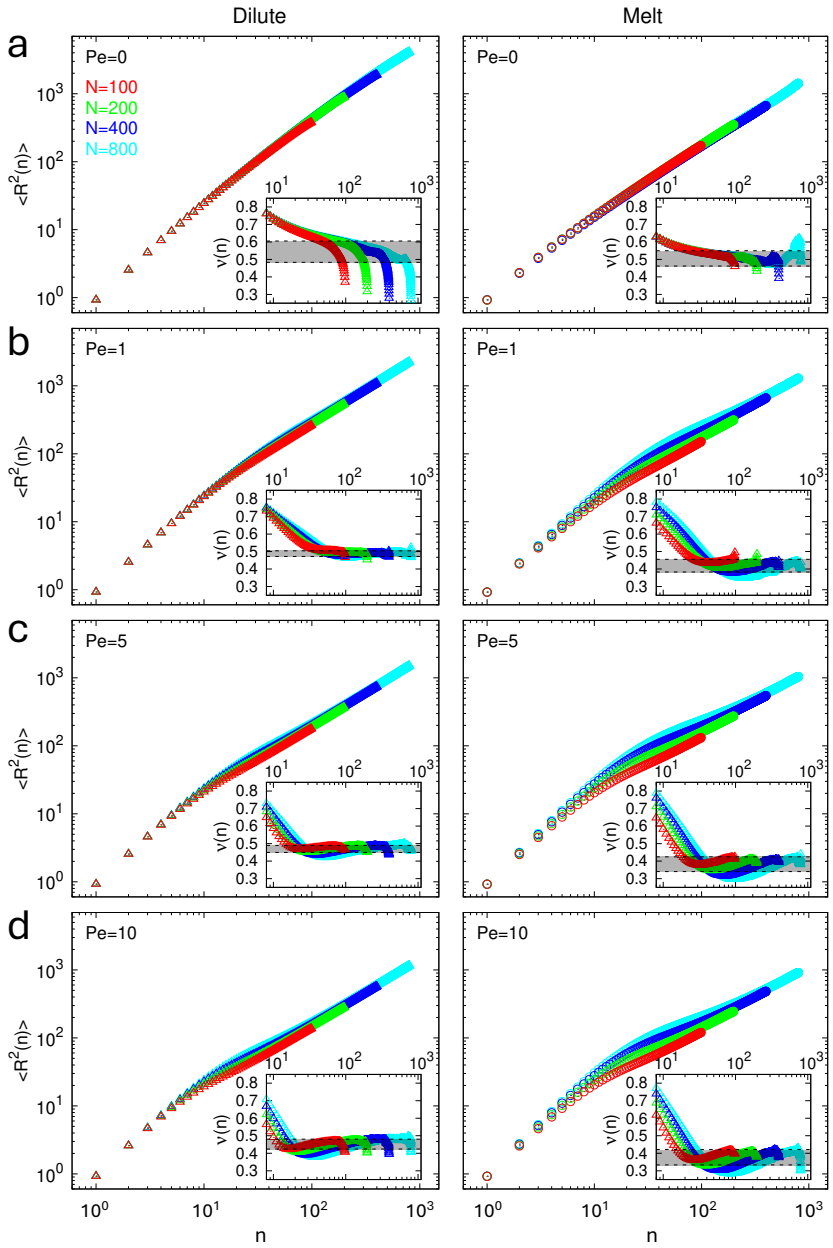

FIG. S1. Mean-square internal distance, $\langle R^2(n)\rangle$ (Eq. (1) in the main text) as a function of contour length separation, n, for dilute (l.h.s. panels, symbols "△") and melt (r.h.s. panels, symbols "○") systems. Increasing Péclet numbers are from top to bottom (for Pe = 20 see Fig. 1(a) in the main text), while different colors are for different total chain lengths N (see legend). (Insets) Local scaling exponent $\nu(n)$ (Eq. (2) in the main text); the shadowed strip denotes the mean scaling exponent and uncertainty, $\bar{\nu} \pm \Delta\nu$ (see values in Table S1). In particular, for Pe = 0 the obtained $\bar{\nu}$'s are coherent with the well known textbook [9] values $\nu = 0.588$ (dilute) and $\nu = 0.5$ (melt), see also caption of Table S1 for more details.

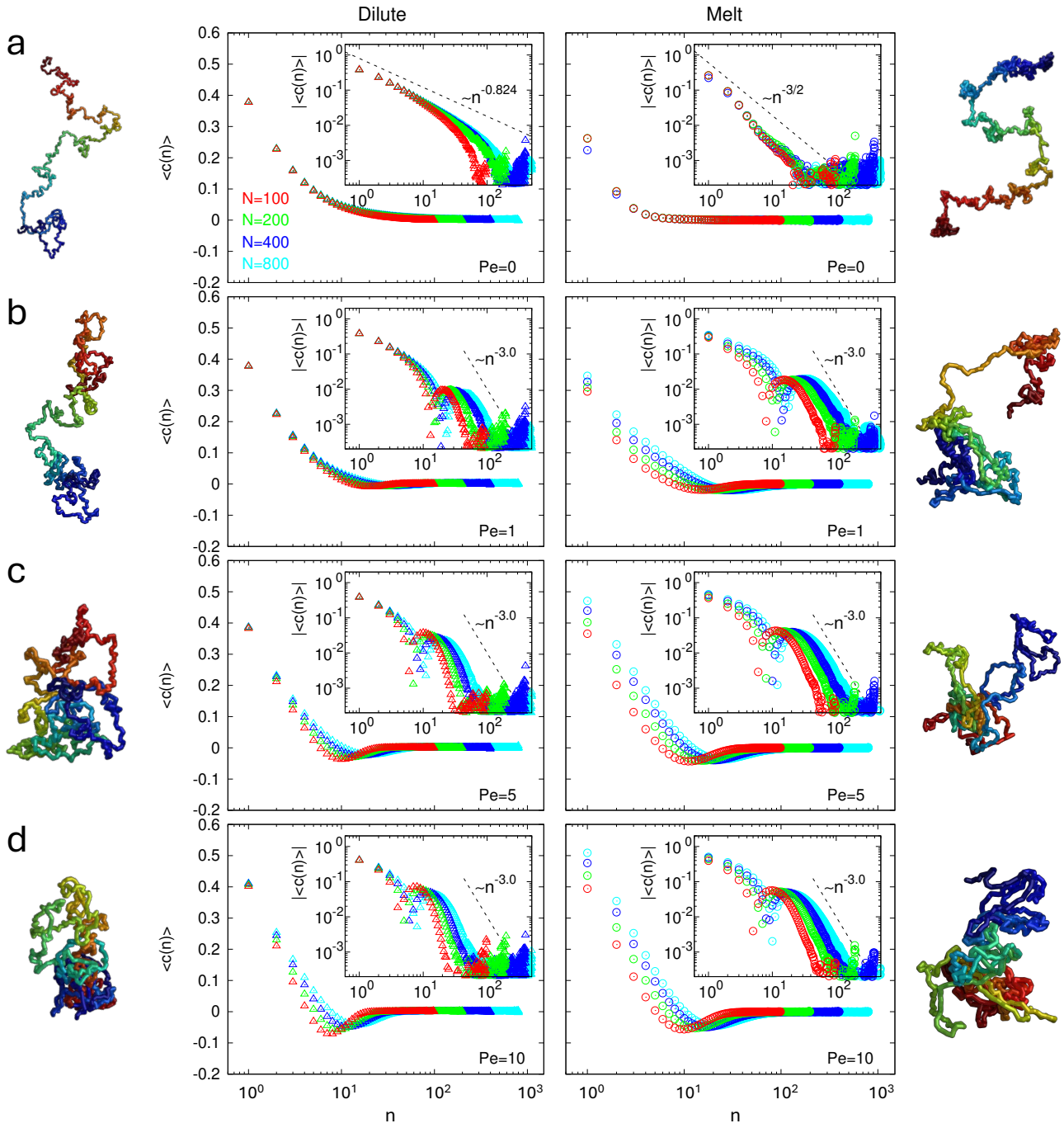

FIG. S2. Bond-vector correlation function, $\langle c(n)\rangle$ (Eq. (3) in the main text), as a function of contour length separation, n, in log-lin representation (main panels) and corresponding norm, $|\langle c(n)\rangle|$, in log-log representation (insets). Power-law decays in the "Pe = 0"-insets correspond to the known [10] behaviors in dilute and melt polymers. The "$\sim n^{-3}$"-decay for active systems (Pe > 0, for Pe $= 20$ see Fig. 1(b) in the main text) is for guiding the eye and purely indicative. Panels ordering, symbols and color code are as in Fig. S1. For dilute and melt conditions and for each Pe, a putative single-chain conformation for $N = 800$ is shown to the side of the corresponding panel (conformations for Pe $= 20$ are shown in Fig. 1(c) in the main text).

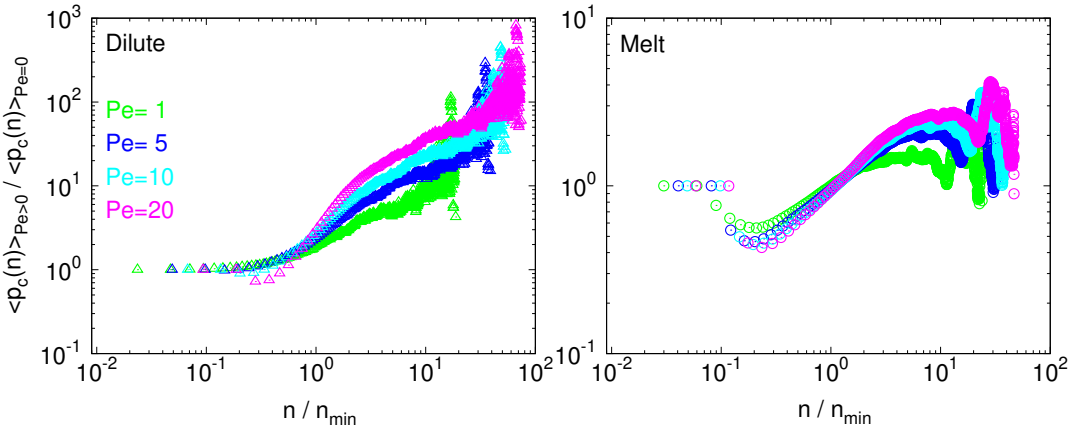

FIG. S3. Mean contact probability $\langle p_c(n)\rangle \equiv \langle \Theta(r_c - |\vec{r}_{n'+n} - \vec{r}_{n'}|)\rangle$, where $\Theta(x)$ is the Heaviside function and $r_c = 2\sigma$ is the conventional cut-off length chosen for contacts' definition. Results for Péclet number $\mathrm{Pe} > 0$ normalized by the corresponding data for passive systems ($\mathrm{Pe} = 0$) as a function of $n/n_{\min}$ and for chains of total length $N = 800$. The plots demonstrate contact enrichments (and, therefore, *looping*) for contour lengths larger than $n_{\min}$.

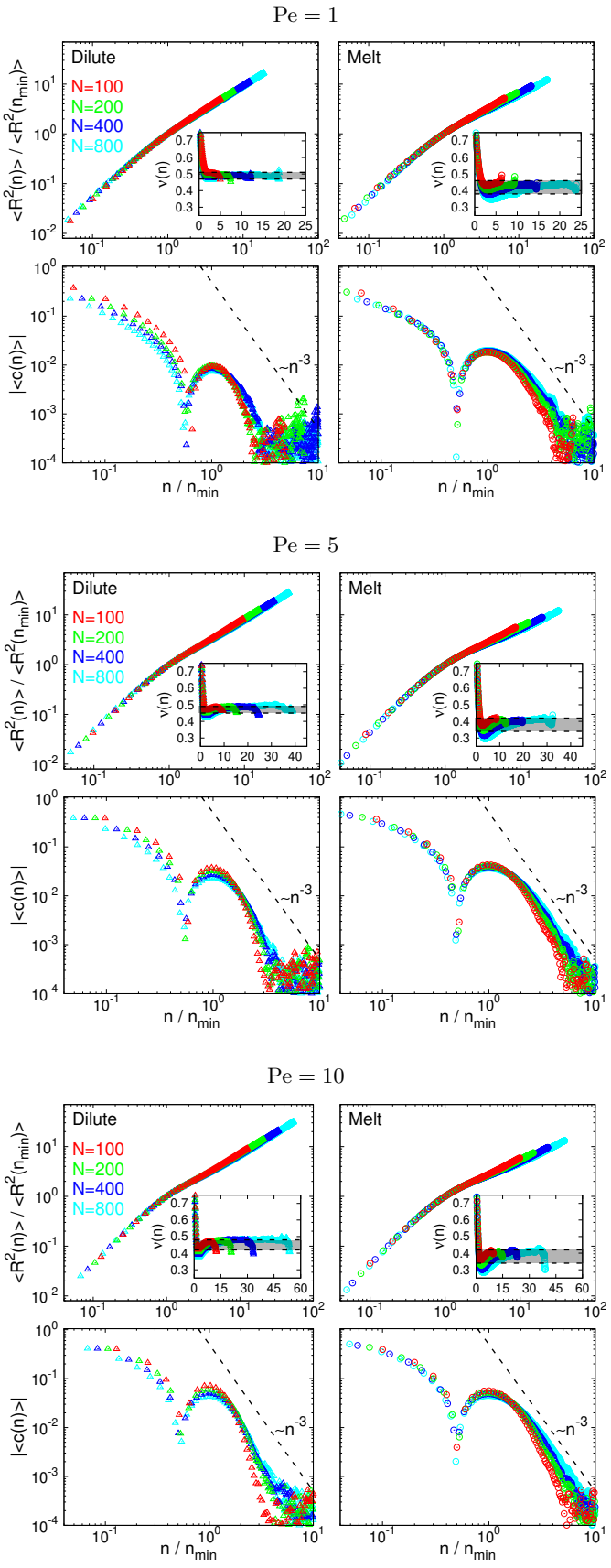

FIG. S4. Normalized mean-square internal distance, $\langle R^2(n)\rangle/\langle R^2(n_{\rm min})\rangle$ (Eq. (1) in the main text), and norm of the bond-vector correlation function, $\langle c(n)\rangle$ (Eq. (3) in the main text; the asymptotic $\sim n^{-3}$-decay is a guide to the eye and purely indicative), as a function of normalized contour length separation, $n/n_{\rm min}$. (Insets) Local scaling exponent $\nu(n)$ (Eq. (2) in the main text) as a function of $n/n_{\rm min}$; the shadowed strip denotes the mean scaling exponent and uncertainty, $\bar{\nu}\pm\Delta\nu$ (see values in Table S1). Results for Péclet numbers Pe = 1, 5, 10 (for Pe = 20, see Fig. 2 in the main text).

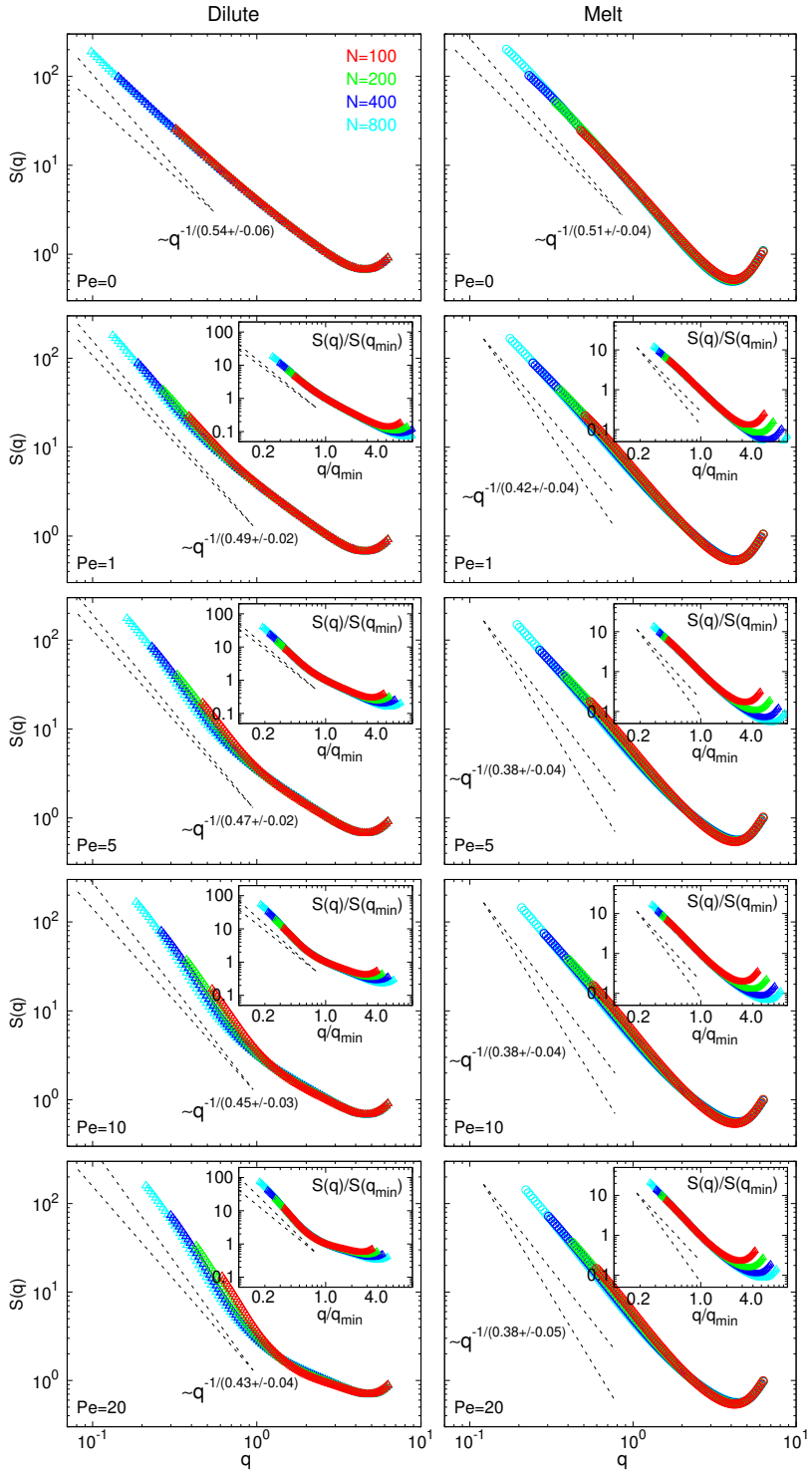

FIG. S5. Single-chain form factor, $S(\vec{q}) = \frac{1}{N}\sum_{i,j=1}^{N}\left\langle e^{i\vec{q}\cdot(\vec{r}_i-\vec{r}_j)}\right\rangle$, as a function of the norm of the wave vector $q = |\vec{q}| \in \left[\frac{2\pi}{\sqrt{\langle R^2_{\rm ee}\rangle}}, \frac{2\pi}{\sigma}\right]$ where $\langle R^2_{\rm ee}\rangle$ is the mean-square end-to-end distance of the polymer (see Fig. S6). Panels from top to bottom are for different Péclet numbers Pe. For Pe = 0, data from different N's collapse onto the same master curve *at all q's*, and $S(q) \sim q^{-1/(\bar{\nu}\pm\Delta\nu)}$ with $\bar{\nu}$ and $\Delta\nu$ as in Table S1. For Pe > 0 and $q < q_{\rm min} \equiv \frac{2\pi}{\sqrt{\langle R^2(n_{\rm min})\rangle}}$ (*i.e.*, large spatial scales), data from different N's obey the, more complicate, single power-law behavior $S(q) \sim S(q_{\rm min})\left(\frac{q}{q_{\rm min}}\right)^{-1/(\bar{\nu}\pm\Delta\nu)}$ (insets), with $\bar{\nu}$ and $\Delta\nu$ as in Table S1. The plots of this figure complement and confirm the results for mean-square internal distances $\langle R^2(n)\rangle$ of Figs. 1 and 2 in the main text and Figs. S1 and S4.

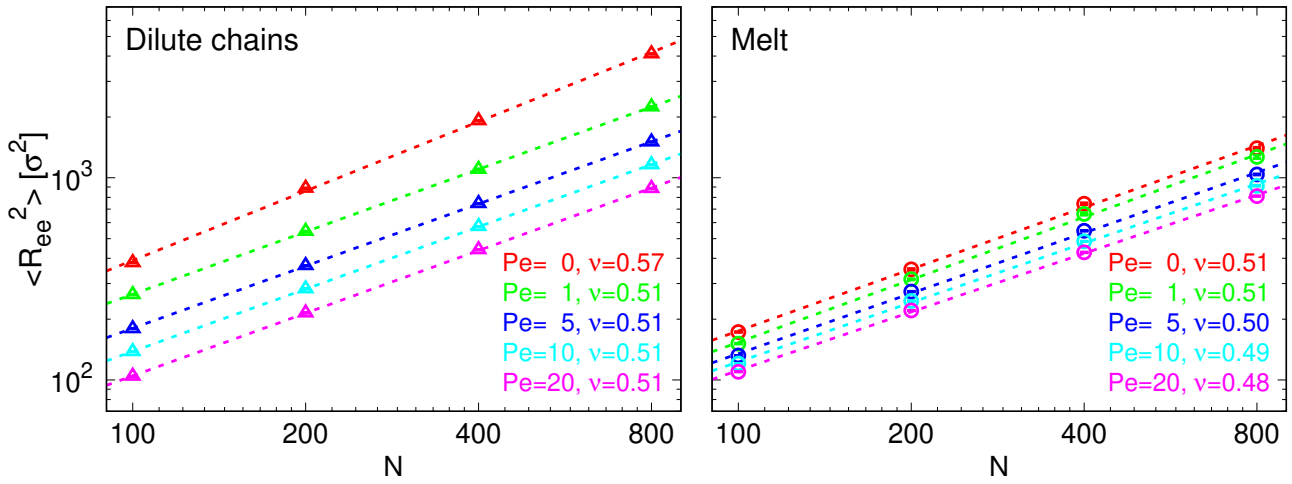

FIG. S6. Polymer mean-square end-to-end distance, $\langle R_{\rm ee}^2 \rangle$ (Eq. (1) in the main text, with $n = N - 1$), as a function of the total chain contour length N and Péclet number Pe. Dashed lines are best fits to simple power-law behavior $= b^2 N^{2\nu}$ (results in the legends). The estimated ν's for Pe = 0 (*i.e.*, for passive systems) are in good agreement with the well known textbook values $\nu = 0.588$ (dilute) and $\nu = 0.5$ (melt), see Ref. [9].

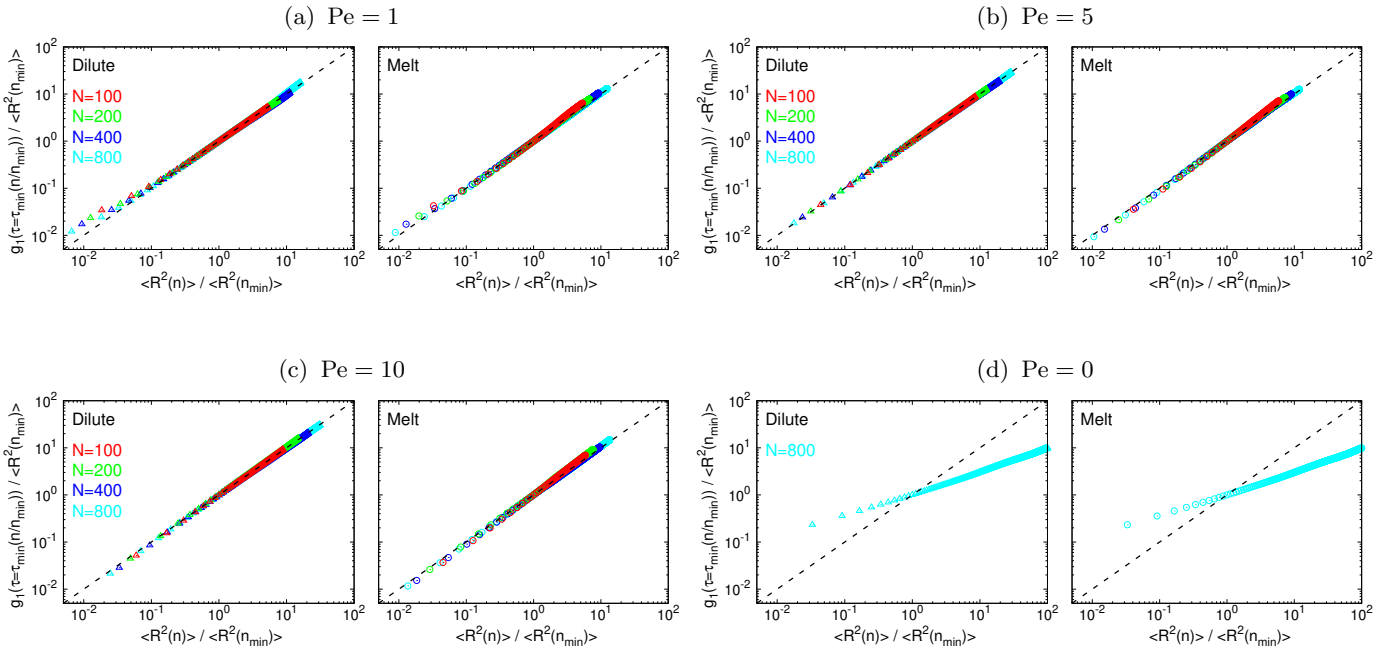

FIG. S7. Parametric plots (symbols) showing the normalized monomer mean-square displacement, $g_1(\tau)/\langle R^2(n_{\rm min})\rangle$ (Eq. (5) in the main text), calculated for $\tau = \tau_{\rm min}(n/n_{\rm min})$ as a function of the normalized mean-square internal distance, $\langle R^2(n)\rangle/\langle R^2(n_{\rm min})\rangle$ (Eq. (1) in the main text). The dashed lines correspond to $y = x$. Panels (a)-(c): Results for Péclet numbers Pe = 1, 5, 10 (for Pe = 20, see Fig. 4 in the main text). Panel (d): Results for passive systems with $N = 800$ and for the same $n_{\rm min}$ from simulations with Pe = 20.

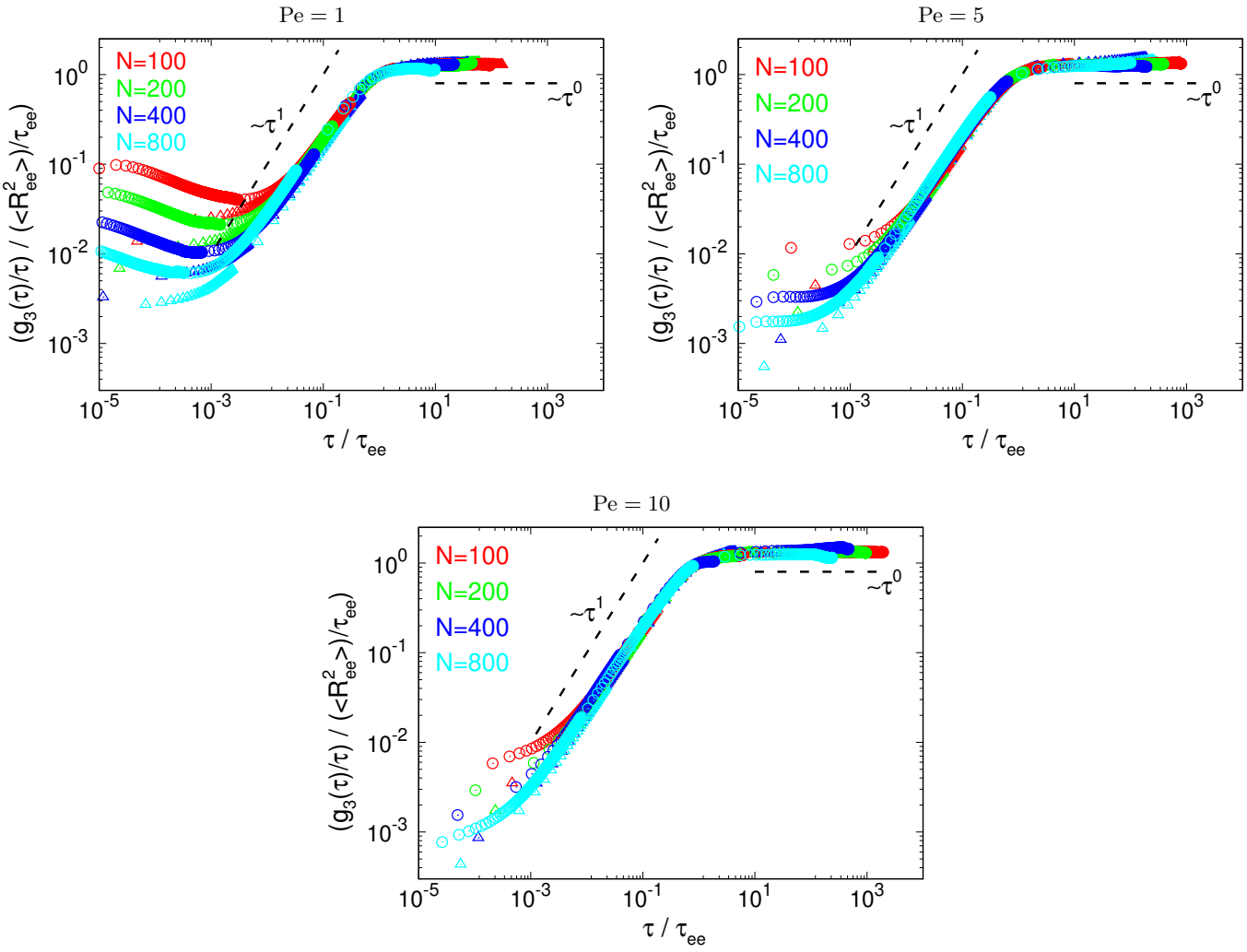

FIG. S8. Mean-square displacement of the chain centre of mass per unit time, $g_3(\tau)/\tau$, normalized by $\langle R_{ee}^2\rangle/\tau_{ee}$ as a function of normalized time τ/τ_{ee}. Results for polymers in dilute (△) and melt (○) conditions, for different contour lengths N (see legend) and for Péclet numbers Pe = 1, 5, 10 (for Pe = 20, see Fig. 5(a) in the main text).

	Dilute					Melt				
Pe	$N = 100$	$N = 200$	$N = 400$	$N = 800$	$\bar{\nu} \pm \Delta\nu$	$N = 100$	$N = 200$	$N = 400$	$N = 800$	$\bar{\nu} \pm \Delta\nu$
0	0.56 ± 0.06	0.56 ± 0.06	0.54 ± 0.05	0.52 ± 0.05	$\mathbf{0.54 \pm 0.06}$	0.51 ± 0.01	0.50 ± 0.01	0.50 ± 0.01	0.51 ± 0.04	$\mathbf{0.51 \pm 0.04}$
1	0.50 ± 0.01	0.488 ± 0.009	0.482 ± 0.009	0.48 ± 0.01	$\mathbf{0.49 \pm 0.02}$	0.44 ± 0.02	0.42 ± 0.02	0.41 ± 0.03	0.40 ± 0.03	$\mathbf{0.42 \pm 0.04}$
5	0.47 ± 0.02	0.47 ± 0.02	0.47 ± 0.02	0.47 ± 0.02	$\mathbf{0.47 \pm 0.02}$	0.40 ± 0.03	0.38 ± 0.03	0.37 ± 0.03	0.37 ± 0.04	$\mathbf{0.38 \pm 0.04}$
10	0.44 ± 0.02	0.45 ± 0.03	0.46 ± 0.03	0.46 ± 0.03	$\mathbf{0.45 \pm 0.03}$	0.39 ± 0.03	0.38 ± 0.03	0.37 ± 0.04	0.37 ± 0.04	$\mathbf{0.38 \pm 0.04}$
20	0.42 ± 0.04	0.43 ± 0.04	0.44 ± 0.04	0.45 ± 0.04	$\mathbf{0.43 \pm 0.04}$	0.38 ± 0.03	0.37 ± 0.04	0.37 ± 0.04	0.38 ± 0.05	$\mathbf{0.38 \pm 0.05}$

TABLE S1. Sequence-average ($\equiv \frac{1}{N-n_{\min}} \sum_{n>n_{\min}} \nu(n)$) of the local scaling exponent $\nu(n)$ for chains of total contour length N and Péclet number Pe; the standard deviation of the data is used for the estimated error bar. The columns with bold fonts report the mean exponent ($\bar{\nu}$) over the different N-values; to account for systematic as well as statistical errors, the relative uncertainty ($\Delta\nu$) is estimated as the square-root of "(spread)^2 + (max-uncertainty-for-different-N's)^2". Values $\bar{\nu} \pm \Delta\nu$ are illustrated as shadowed strips in the insets of Figs. 1(a) and 2(a) in the main text and Figs. S1 and S4 here. For convenience, for Pe = 0 (*i.e.*, for passive chains) we have used the same $n_{\min}$ of Pe = 1; the obtained $\bar{\nu}$ are coherent with the scaling exponents measured by fitting a power-law behavior to the "mean-square end-to-end distance $\langle R_{ee}^2 \rangle$ vs. N" data (and, therefore, with the well known textbook [9] values $\nu = 0.588$ (dilute) and $\nu = 0.5$ (melt), see also Fig. S6 and its caption). Conversely, the obtained estimates for Pe > 0 differ significantly from the corresponding power-law fits to the "$\langle R_{ee}^2 \rangle$ vs. N" data (Fig. S6).

Dilute						
Pe	n_0	α	R_0^2	β	β/α	$\bar{\nu} = \frac{1}{2}\frac{1-\beta}{1-\alpha}$
1	8.2 ± 1.7	0.36 ± 0.02	17.4 ± 4.1	0.45 ± 0.02	1.2 ± 0.1	0.43 ± 0.03
5	3.3 ± 0.2	0.330 ± 0.007	4.9 ± 0.4	0.435 ± 0.006	1.32 ± 0.05	0.422 ± 0.009
10	2.4 ± 0.2	0.311 ± 0.008	3.0 ± 0.3	0.433 ± 0.008	1.39 ± 0.06	0.41 ± 0.01
20	2.4 ± 0.1	0.259 ± 0.005	2.7 ± 0.1	0.396 ± 0.006	1.53 ± 0.05	0.407 ± 0.007

Melt						
Pe	n_0	α	R_0^2	β	β/α	$\bar{\nu} = \frac{1}{2}\frac{1-\beta}{1-\alpha}$
1	5.2 ± 1.6	0.37 ± 0.03	4.7 ± 1.7	0.63 ± 0.02	1.7 ± 0.2	0.30 ± 0.03
5	3.3 ± 0.9	0.37 ± 0.03	2.8 ± 1.3	0.63 ± 0.04	1.7 ± 0.2	0.29 ± 0.04
10	3.1 ± 0.8	0.35 ± 0.02	2.7 ± 1.1	0.59 ± 0.04	1.7 ± 0.2	0.31 ± 0.04
20	2.9 ± 0.5	0.32 ± 0.02	2.6 ± 0.7	0.55 ± 0.03	1.7 ± 0.2	0.33 ± 0.03

TABLE S2. Fit parameters for the empirical power-laws $n_{\min} = n_0 \left(\frac{N}{n_0}\right)^{\alpha}$ and $\langle R^2(n_{\min}) \rangle = R_0^2 \left(\frac{N}{n_0}\right)^{\beta}$ (see Eq. (4) and Eq. (5) in the main text) for dilute and melt systems and Péclet number Pe. The last two columns display the ratios β/α describing the scaling $\langle R^2(n_{\min}) \rangle \sim n_{\min}^{\beta/\alpha}$ and the values for $\bar{\nu}$ (to be compared with the direct results shown in Table S1) predicted by the scaling arguments illustrated in the main text.

[1] V. Bianco, E. Locatelli, and P. Malgaretti, Globulelike conformation and enhanced diffusion of active polymers, Phys. Rev. Lett. **121**, 217802 (2018).

[2] M. Fazelzadeh, E. Irani, Z. Mokhtari, and S. Jabbari-Farouji, Effects of inertia on conformation and dynamics of tangentially driven active filaments, Phys. Rev. E **108**, 024606 (2023).

[3] K. Kremer and G. S. Grest, Dynamics of entangled linear polymer melts: A molecular-dynamics simulation, J. Chem. Phys. **92**, 5057 (1990).

[4] By this choice of the parameters the FENE bond (Eq. (S2)) is made stronger, in this way accidental strand-crossings between chains can be carefully avoided (see Ref. [11]).

[5] A. P. Thompson, H. M. Aktulga, R. Berger, D. S. Bolintineanu, W. M. Brown, P. S. Crozier, P. J. in't Veld, A. Kohlmeyer, S. G. Moore, T. D. Nguyen, *et al.*, Lammps-a flexible simulation tool for particle-based materials modeling at the atomic, meso, and continuum scales, Comput. Phys. Commun. **271**, 108171 (2022).

[6] M. A. Ubertini and A. Rosa, Computer simulations of melts of ring polymers with nonconserved topology: A dynamic monte carlo lattice model, Phys. Rev. E **104**, 054503 (2021).

[7] M. A. Ubertini, J. Smrek, and A. Rosa, Entanglement length scale separates threading from branching of unknotted and non-concatenated ring polymers in melts, Macromolecules **55**, 10723 (2022).

[8] Note that, only for the preparation of the initial states, we have adopted the conventional [3] Kremer-Grest values for the parameters in Eq. (S2), namely: $\epsilon = 1\,\kappa_B T$ and $k = 30\,\kappa_B T/\sigma^2$.

[9] M. Rubinstein and R. H. Colby, *Polymer Physics* (Oxford University Press, New York, 2003).

[10] J. P. Wittmer, H. Meyer, J. Baschnagel, A. Johner, S. Obukhov, L. Mattioni, M. Müller, and A. N. Semenov, Long range bond-bond correlations in dense polymer solutions, Phys. Rev. Lett. **93**, 147801 (2004).

[11] E. Locatelli, V. Bianco, and P. Malgaretti, Activity-induced collapse and arrest of active polymer rings, Phys. Rev. Lett. **126**, 097801 (2021).